# OPTIMAL DESIGN OF A VIBRATION-BASED ELECTROMAGNETIC ENERGY HARVESTER USING A SIMULATED ANNEALING ALGORITHM

**M.-C. Chiu** *

*Department of Mechanical and Automation Engineering*
*Chung Chou University of Science and Technology*
*Changhua, Taiwan 51003, R.O.C.*

**Y.-C. Chang** **L.-J. Yeh** **C.-H. Chung**

*Department of Mechanical Engineering*
*Tatung University*
*Taipei, Taiwan 10452, R.O.C.*

## ABSTRACT

This paper presents the optimal design of an electromagnetic vibration-based generator using the simulated annealing method (SA). To optimally extract the vibrational energy of a system vibrating at a specific frequency, the selected mass and spring stiffness of a resonant vibration is required. The relationship between induced energy and the generator's structure, its permanent magnet height and diameter, number of turns, and wire diameter in a single air coil are discussed. Also, a prototype of the vibration-based electrical generator is built and tested via a shaker excited at resonance frequency and input amplitude of 0.06mm. Consequently, results reveal that the design parameters (permanent magnet height and diameter, number of turns, and wire diameter) play essential roles in maximizing electrical power.

**Keywords:** Electromechanical generator, Permanent magnet machine, Optimization.

## 1. INTRODUCTION

There has been substantial research of vibration energy used for electrical generation. Energy transformation results in three types of electrical generation — electromagnetic transduction, electrostatic transduction, and piezoelectric transduction [1,2]. The structure of the device is of two types — the cantilever beam system [3-6,22] and the spring-mass system [7-11]. Some structures are fit for lower frequencies, and some are fit for higher frequencies. For a structure with a cantilever beam with reciprocating motion, a higher displacement beyond the elastic limit will result in fatigue and induce damage. Because of this, application of the cantilever-beam electrical generator is limited to small vibrations at a higher frequency and is used within small systems such as the MEMS [18]. A structure with a spring-mass system is often used to extract energy from a vibration system of lower frequencies and larger displacement. Of course, research on mathematical models for a vibration-based electrical generation system has been addressed [12,19]. However, mechanism design and parameter analysis for a real vibration-based electrical generation system has been neglected. The optimization of electrical power for a space-limited electrical generator has also been overlooked.

In this paper, the mathematical model for a vibration-based electro-mechanical generator will be established. In addition, the sensitivity of electronic generation with respect to various design parameters will also be assessed. Moreover, a prototype of a spring-mass electrical generator will be constructed. The accuracy of the theoretical model with a real damping ratio will be checked using experimental data. Thereafter, the optimization of design parameters such as the diameter of the magnet ($d_m$), the length of the magnet ($l_m$), the number of coil turns ($N$), the diameter of the coil ($D_c$), and the diameter of the coil wire ($d_w$) will be processed using a simulated annealing algorithm (SA) [15,16]. Maximum electrical voltage will be achieved by using optimally designed parameters when applying the SA with various resonant frequencies. For a system vibrating with a specific frequency, the related mass and spring stiffness will be appropriately selected to meet the resonant vibration. The induced electrical voltage will be closely related to the shape of the vibrator and the coil allocation. Consequently, this paper provides a quick and effective method to maximize the induced electrical voltage by optimally designing a shaped magnet and coil within a limited space.

* Corresponding author (minchie.chiu@msa.hinet.net)


DOI : 10.1017/jmech.2012.104
Copyright © 2012 The Society of Theoretical and Applied Mechanics, R.O.C.
https://doi.org/10.1017/jmech.2012.104 Published online by Cambridge University Press

## 2. MATHEMATICAL MODELS

The vibration-based electromagnetic energy harvester shown in Fig. 1 transforms mechanical energy into electrical power via a resonant vibrating system. The coupled electromechanical system includes a permanent magnet that is in a reciprocating motion. Based on Faraday's law of electromagnetic induction and Lenz's law, the outputted electrical power of the coil is proportional to the magnetic flux variance. Therefore, the magnetic intensity at different locations will be predicted via the mass's kinetic motion and the density distribution of the static magnetic field. Moreover, the electrical voltage will be induced via the corresponding position of the coil and magnet. The mathematical model for a single degree of a free mechanical vibrational system as well as electrical power induced by the magnetic flux variance is shown below.

### 2.1 Motion of the One-Mass Vibration System

A single degree of the free mechanical vibration system is depicted in Fig. 2(a). The free-body diagram for a single degree of the free vibration system is also shown in Fig. 2(b). Based on Fig. 2(b), the equation of motion using Newton's second law is

$$m\ddot{z}_1 + c_{sys}(\dot{z}_1 - \dot{z}_o) + k_{sys}(z_1 - z_o) = 0 \tag{1a}$$

where

$$c_{sys} = c_m + c_e \tag{1b}$$

According to Stephen [12], $c_e$, the damping coefficient due to the coil effect is

$$c_e = \frac{K^2}{R_{load} + R_{iner}} \tag{2a}$$

where

$$K = NBl \;;\; R_{iner} = \rho_c \frac{l_c}{A_c} \;;\; A_c = \frac{\pi d_w^2}{4} \tag{2b}$$

Assuming that the base is harmonically excited, it yields

$$z_o = Y\sin(\omega \cdot t) \tag{3}$$

Let the relative displacement $z$ be

$$z = z_1 - z_o \tag{4}$$

Plugging Eq. (3) and (4) into Eq. (1) yields

$$m\ddot{z} + c_{sys}\,\dot{z} + k_{sys}\,z = m\omega^2 Y\sin(\omega \cdot t) \tag{5}$$

The steady-state solution of Eq. (5) is

$$z(t) = Z\sin(\omega t - \phi) \tag{6a}$$

where

$$Z = \frac{mY\omega^2}{\left[(k - m\omega^2)^2 + c_{sys}^2\,\omega^2\right]^{1/2}} \tag{6b}$$

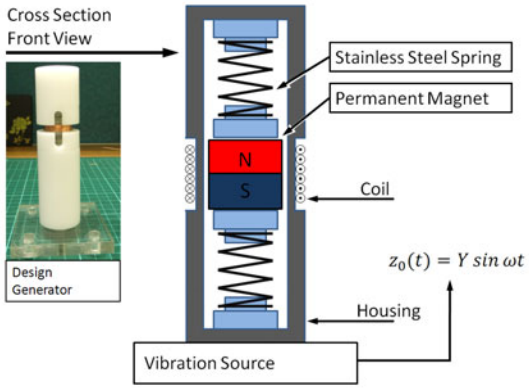



Fig. 1 A prototype of a vibration-based electromagnetic energy harvester

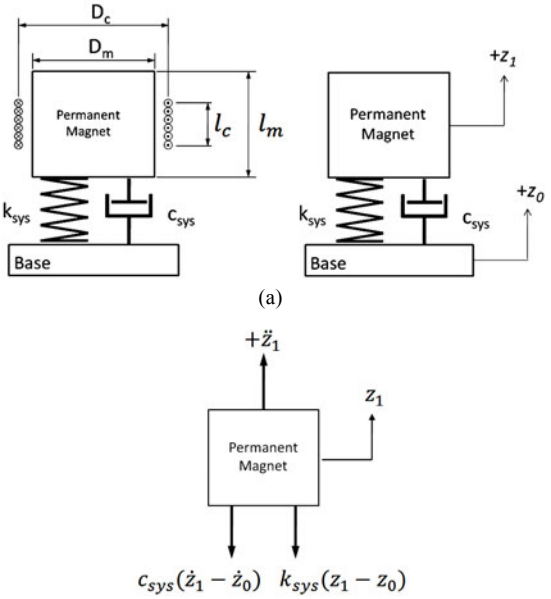



Fig. 2 A base-excitation model

$$\phi = \tan^{-1}\left(\frac{c_{sys}\,\omega}{k - m\omega^2}\right) \tag{6c}$$

### 2.2 The Magnetic Flux for a Permanent Magnet

For the cylindrical permanent magnet, assuming that the inner magnetization is uniform, the coupled-currents method is applied for calculating the magnetic field of the permanent magnet [20]. The effective current distribution will be the same as an ideal solenoid. Considering the magnetic field along the z-axis and applying the Biot-Savart law yield

$$\int d\vec{B}_z = \int_{-\frac{l_m}{2}}^{\frac{l_m}{2}} \int_0^{2\pi} \frac{\mu_0 I}{4\pi r_1^2}\left(\frac{\sin\theta_1 - \sin\theta_2}{r_1^2 - r_2^2}\right) R\,d\theta\,dz(\hat{u}_\phi \times \hat{r}) \tag{7a}$$

where



https://doi.org/10.1017/jmech.2012.104 Published online by Cambridge University Press

$$R=\frac{d_m}{2},\ r_1=\sqrt{\left(z+\frac{l_m}{2}\right)^2+\frac{d_m^2}{4}},\ r_2=\sqrt{\left(z-\frac{l_m}{2}\right)^2+\frac{d_m^2}{4}} \tag{7b}$$

Consequently, the distribution flux density through the center of cylindrical axis is [11].

$$B_z(z)=B_r\left[\frac{z+\frac{l_m}{2}}{\sqrt{4\left(z+\frac{l_m}{2}\right)^2+d_m^2}}-\frac{z-\frac{l_m}{2}}{\sqrt{4\left(z-\frac{l_m}{2}\right)^2+d_m^2}}-g\right] \tag{7c}$$

where

$$\begin{cases} g=1 & \left(-\frac{l_m}{2}<x<\frac{l_m}{2}\right) \\ g=0 & \left(-\frac{l_m}{2}>x,\ x>\frac{l_m}{2}\right) \end{cases} \tag{7d}$$

A NdFeB-made (Type N35) cylindrical permanent magnet with a diameter of 12mm, a height of 10mm, and the residual flux density $B_r$ of 1.2T is adopted. According to the data sheet from the manufacturer, the related magnetic flux density distribution is shown in Fig. 3. In addition, Fig. 3 also indicates that magnetic vector field starts to change the direction of other components at a center where $z=\pm 1$. Moreover, according to Faraday's law, the induced voltage will be proportional to the changes of the magnetic flux rate. Therefore, the allocation of the coil can be considered to be preset at the place that has the maximum variation of the magnetic flux.

### 2.3 The Electromagnetic Energy Output

According to Wang's analysis [21] and experimental work, the best allocation of the coil will be obtained, and the magnetic voltage will increase if the layer of the coil increases. Currently, to simplify the analysis, only a one layer solenoid/ winding coil is considered. Moreover, the magnet will be allocated at the center of the coil. Based on Faraday's law, the individual induced voltage for each circular coil is

$$\varepsilon=-\frac{d\phi}{dt}=-A\frac{dB_z(z)}{dz}\cdot\frac{dz}{dt} \tag{8a}$$

where

$$A=\frac{\pi d_c^2}{4}$$

$$\frac{dB_z(z)}{dz}=B_r\left[\frac{d_m^2}{\sqrt{\left[4\left(z+\frac{l_m}{2}\right)^2+d_m^2\right]^3}}-\frac{d_m^2}{\sqrt{\left[4\left(z-\frac{l_m}{2}\right)^2+d_m^2\right]^3}}\right] \tag{8b}$$

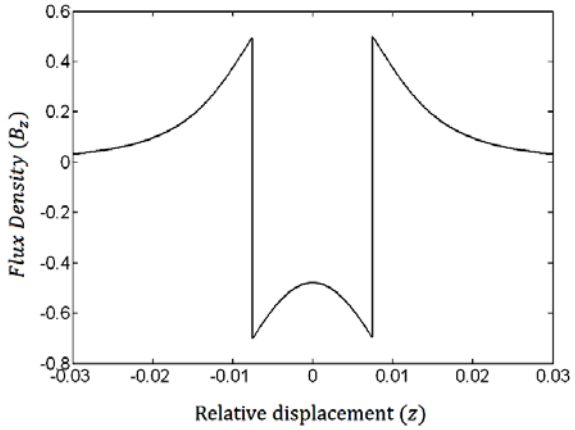



Fig. 3 Magnetic flux density distribution at $z$-axis

Summing up all the coil's induced electrical voltages, the total voltage induced by a moving magnet is

$$V_{total}=\sum_{n=0}^{N-1}\varepsilon_n \tag{9}$$

### 2.4 Objective Function

To optimally design a compact vibration-based electromagnetic energy harvester, an objective function for harvesting electromagnetic energy per unit mass is

$$Obj_1(d_m,\ l_m,\ N,\ d_w)=V_{\text{total}}^2/(R\cdot m) \tag{10}$$

## 3. MODEL CHECK

To verify the accuracy of the mathematical model and experimental data, the experimental work of a vibration-based electromagnetic energy harvester in conjunction with a vibrating source shown in Fig. 4 has been established. As indicated in Fig. 4, a NdFeB-made cylindrical permanent magnet serves as a vibrator. The vibrator that has a 12mm diameter and is 10mm in height is compressed by two springs (Stainless A313) at both ends. The selected spring is 24mm in $l_s$ (free length of the spring), 0.5mm in $d_s$ (diameter of the spring's wire), 24mm in $D_s$, and 6 turns of $N_a$ (available turns of a spring). The housing of the vibration-based electromagnetic energy harvester is made of Polyoxymethylene (POM) and Polymethylmethacrylate (PMMA).

Because of the higher flux density near the magnet, the coil will be closely allocated to the magnet's surface. The coil's diameter ($D_c$) includes the $d_m$ (the magnet's diameter) and a 5mm gap. The height of the coil ($l$) is half the length ($l_m$). In order to reduce the extra damping force induced by air resistance when the mass is moving within the tube, the venting holes at both the upper end and side are provided.

Before the theoretical formula is calculated, some physical conditions will be preset and experimentally measured. The physical conditions are given and shown in Table 1. As indicated in Fig. 5, to obtain the spring's stiffness and damping ratio, experimental work using the logarithmic decrement method in conjunction with a piezoelectric pressure sensor is carried out.



https://doi.org/10.1017/jmech.2012.104 Published online by Cambridge University Press

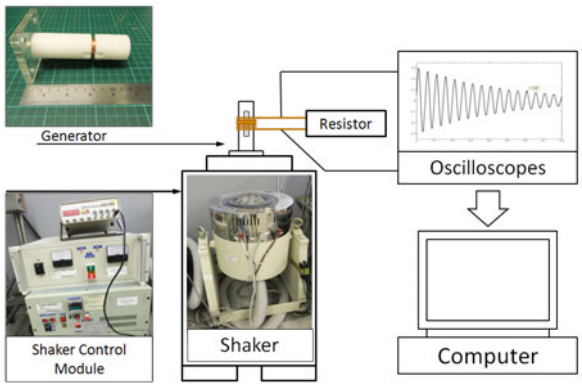



Fig. 4 Experimental equipment for a vibration-based electromagnetic energy harvester

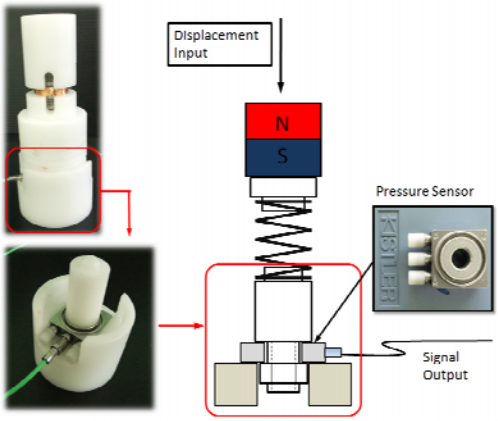


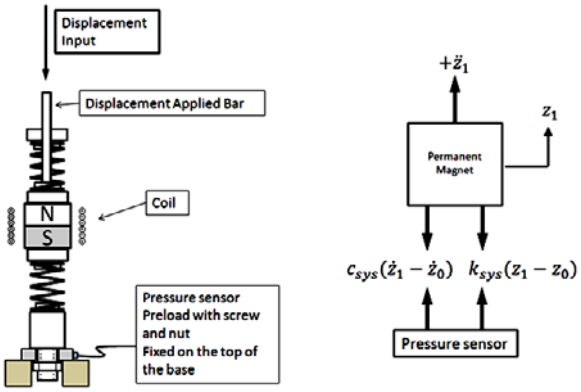

Fig. 5 Device used to measure both the damping ratio and spring constant

Table 1 Ranges of the design parameters used in the SA optimization

| Design parameter | Range of design parameter |
|---|---|
| Length of Magnet - $l_m$ | 5 ~ 50 mm |
| Diameter of Magnet - $D_m$ | 5 ~ 50 mm |
| Number of turns - $N$ | 10 ~ 500 |
| Wire diameter - $d_w$ | 0.1 ~ 1 mm |
| Input Frequency - $f_{in}$ | [10,20,30] |
| Input Amplitude - $Y$ | 0.1 (mm) |

A pressure sensor is used to detect the force loading on the mass during the vibrating process. As indicated in Fig. 6(a), for experimental step 1, a carbon fiber bar will push the magnet with a small displacement of 2 ~ 3 (mm). For experimental step 2, releasing the mass suddenly, the mass will vibrate freely. The pressure transmitted to the pressure sensor via the mass will be detected.

Based on the free-body diagram shown in Fig. 6(b) and Newton's second law, the force loading of the pressure sensor includes the spring force ($F_s = k_{sys}(z_1 - z_0)$) and the damping force ($F_d = c_{sys}(\dot{z}_1 - \dot{z}_0)$). According to the equation of motion, the velocity will be zero ($\dot{z} = 0$, $F_d = 0$) when the mass is at the highest position. Therefore, the spring force is proportional to the displacement. Here, the pressure




(a) (b)

Fig. 6 The cross section of a device and the free-body diagram

at the pressure sensor will also be linearly proportional to the spring force. Moreover, the system's damping ratio will be obtained by using the logarithmic decrement method.

As indicated in Fig. 7(a), the damping coefficient can be obtained by using an experimental measurement without the coil. Similarly, as indicated in Fig. 7(b), the combined damping ratio of the mechanical and the coil effect will also be measured with the coil. The relationships between the damping ratio and the damping coefficient are listed below:

$$c_{sys} = 2\varsigma_{sys}\sqrt{km} = c_m + c_e = 2\varsigma_m\sqrt{km} + c_e \tag{11a}$$

$$c_e = 2\varsigma_{sys}\sqrt{km} - 2\varsigma_m\sqrt{km} = 2\sqrt{km}(\varsigma_{sys} - \varsigma_m) \tag{11b}$$

The logarithmic, δ, can be calculated using the logarithmic decrement method

$$\delta = \frac{1}{n}\ln\left(\frac{V_o}{V_n}\right) \tag{12}$$

where $V_o$ is the first peak amplitudes and $V_n$ is the $n$-th period peak amplitude. Therefore, the related damping ratio is

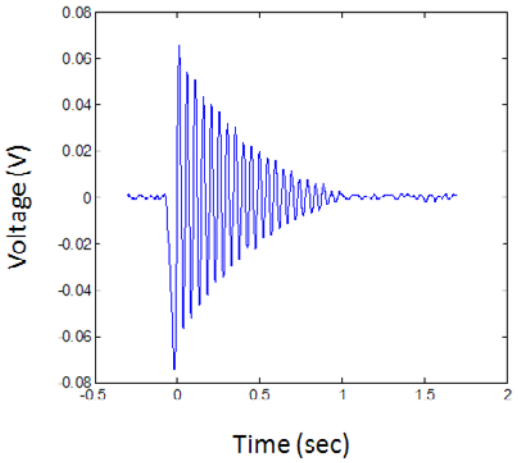
$$\varsigma_{sys} = \frac{1}{\sqrt{1+\left(\frac{2\pi}{\delta}\right)^2}} \tag{13}$$

According to Eq. (13), the resulting system damping ratio ($\varsigma_{sys}$) is 0.016. In addition, by using the experimental $\rho_c$ at $N$ = 200, 300, 400, and 500 turns, the resulting averaged $\rho_c$ is calculated as $6.3 \times 10^{-8}(\Omega \cdot m)$. Plugging the averaged $\rho_c$ into Eq. (2), the theoretical damping ratio ($c_e$) induced by the coil is 0.0019 (N·s/m).

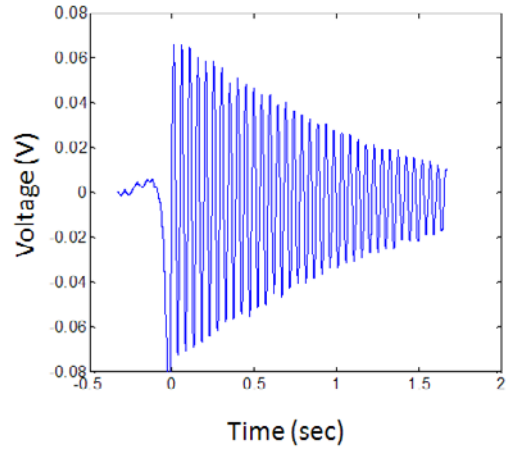
To verify the accuracy of the theoretical damping ratio ($c_e$) in Eq. (2), experimental work has been performed and compared with the theoretical data. As indicated in Fig. 8, the accuracy of the damping ratio ($c_e$) is reliable. Therefore, the mechanical damping coefficient ($c_m$) can be obtained. Using the above data in the theoretical



https://doi.org/10.1017/jmech.2012.104 Published online by Cambridge University Press




(a) 500 turns




(b) 0 turns

Fig. 7 Experimental result of a pressure sensor signal induced by a natural vibration

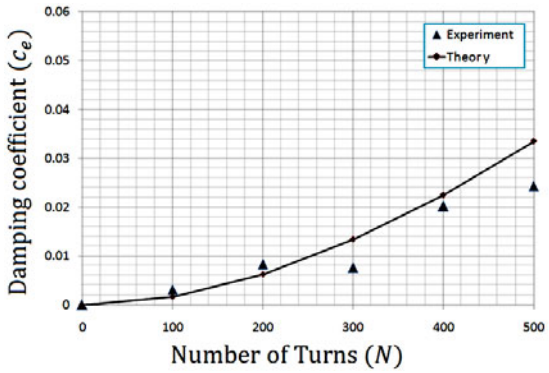



Fig. 8 Number of coil turns ($N$) with respect to the coil's damping coefficient

calculation, the profile of the theoretically induced electrical voltage and the experimental voltage with respect to frequency is obtained and shown in Fig. 9. Because the center axis of the helical spring, the center axis of cylindrical magnet, and the center axis of the vibration source may not be set up on the same line, some vibrational energy might be dissipated at the un-axial direction. Therefore, the practical energy detected in the experimental work will be smaller than that of the theoretical prediction. The peak-to-peak value of the induced voltage in different excited frequencies is shown in Fig. 10.

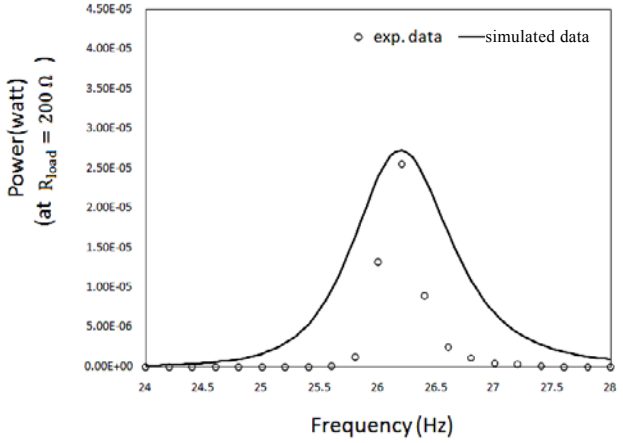



Fig. 9 Performance of a vibration-based electromagnetic energy harvester when comparing the theoretical simulation and the experimental work

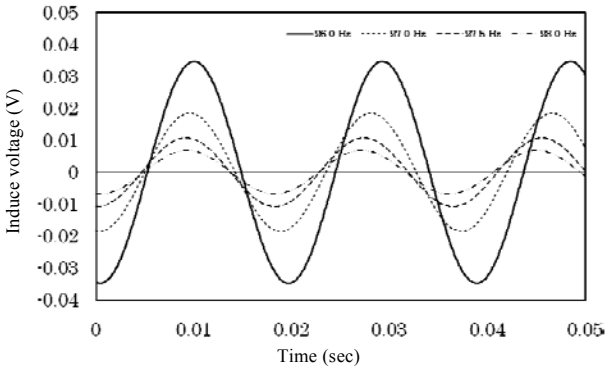



Fig. 10 Peak-to-peak value of the induced voltage in different excited frequencies

As depicted in Fig. 9, the performance curve of the theoretical and experimental data are in agreement. Moreover, the maximum electromagnetic voltage is tuned around the desired frequency of 26Hz. Therefore, the mathematical model is acceptable. Consequently, the model linked by the SA numerical method is used for optimizing the unit induced electrical voltage of a single degree of the free vibration-based electromagnetic energy harvester in the following section.

## 4. SENSITIVITY ANALYSIS

The related design parameters have been selected based on the experimental study by varying the individual parameter step by step. Moreover, to verify the validity of the design parameters, the sensitivity analysis (numerically plotting the electricity power with respect to the parameters) has been carried out and is described below:

### 4.1 Energy Density with Respect to the Diameter of a Cylindrical Permanent Magnet and the Number of Coil Turns

Assuming that the height of a cylindrical permanent magnet is 20mm, the input base-excitation frequency is 26Hz, displacement amplitude (Y) is 0.1mm, the load-



https://doi.org/10.1017/jmech.2012.104 Published online by Cambridge University Press

ing resistor is 200Ω, and the mechanical damping coefficient is 0.028905N·sec/m. A response curve between the energy density ($OBJ_1$) with respect to the diameter of a cylindrical permanent magnet ($d_m$) and the number of coil turns ($N$) is assessed and shown in Fig. 11. As indicated in Fig. 11, the peak value of the energy density ($OBJ_1$) will occur at the lower $d_m$ when $N$ decreases.

### 4.2 Energy Density with Respect to the Number of Oil Turns and the Excited Displacement Amplitude

The relationship between the energy density ($OBJ_1$) and the number of coil turns ($N$) at various excited displacement amplitudes (Y) has been investigated and shown in Fig. 12. As indicated in Fig. 12, the peak value of the energy density will increase, and its profile will shift to a higher number of coil turns ($N$) when the excited displacement amplitude increases.

### 4.3 Energy Density with Respect to the Number of Coil Turns and the Diameter of the Coil Wire

In the case of a magnet with a diameter of 27mm, a height of 50mm, an excited frequency of 26Hz, and an excited displacement amplitude of 0.1mm, the relationship between the energy density ($OBJ_1$) and the number of coil turns ($N$) at various coil wire diameters is shown in Fig. 13. As indicated in Fig. 13, the peak value of the energy density will increase and its profile will be shifted to a higher number of coil turns ($N$) when the diameter of the coil's wire ($d_w$) decreases.

### 4.4 Energy Density with Respect to the Magnet'S Height and Diameter

The response curve of the energy density ($OBJ_1$) with respect to the magnet's height ($l_m$) and diameter ($d_m$) is shown in Fig. 14. As indicated in Fig. 14, an optimum value occurs in the profile.

Consequently, the results in Figs. 11 ~ 14 indicate that the response of the energy density ($OBJ_1$) with respect to the coil turns ($N$), the magnet's height ($l_m$), the diameter ($d_m$), and the coil wire ($d_w$) is very sensitive. Therefore, the above parameters will be adopted in the shape optimization of the vibration-based electrical generator in the following section.

## 5. CASE STUDIES

Three kinds of base vibrating sources (excited frequencies of 10Hz, 20Hz, and 30Hz) with the same displacement amplitude of 0.1mm are proposed. To optimally extract these vibrations using a spring-mass electromagnetic energy harvester, four kinds of design parameters — the coil turns ($N$), magnet's height ($l_m$), diameter ($d_m$), and the coil wire ($d_w$) — in conjunction with the SA method are assessed in the flowing sections. The related ranges of the design parameters are shown in Table 1. Moreover, the given data for the vibrating system and the vibration-based electromagnetic energy harvester is shown in Table 2.

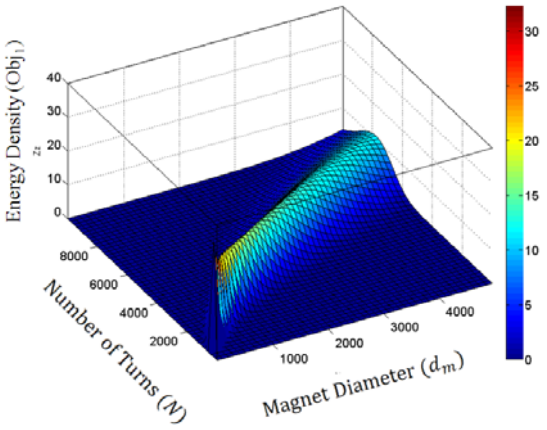



Fig. 11 Energy density ($OBJ_1$) with respect to the number of coil turns ($N$) and the diameter of the magnet ($d_m$)

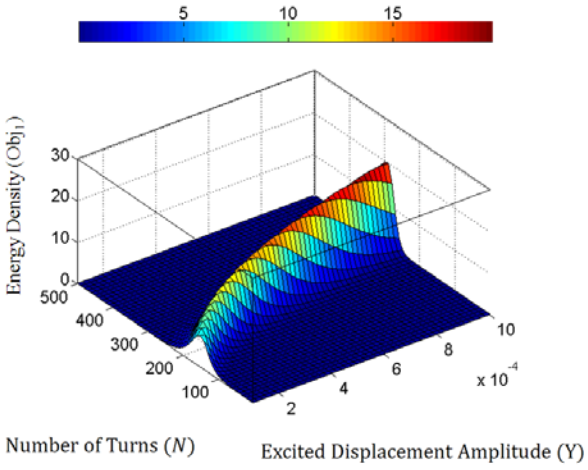



Fig. 12 Energy density ($OBJ_1$) with respect to the number of coil turns ($N$) for various excited displacement amplitudes

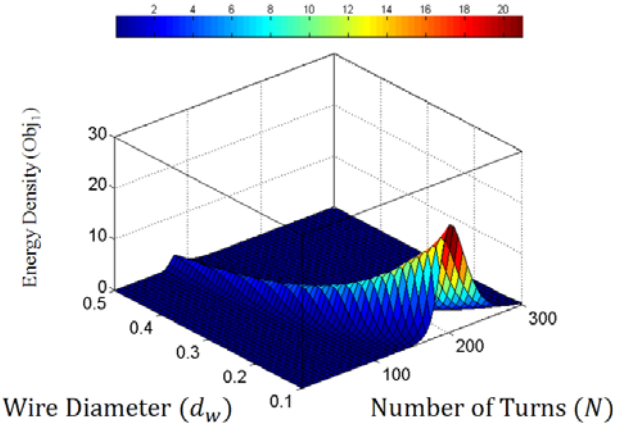



Fig. 13 Energy density ($OBJ_1$) with respect to the coil wire diameter ($d_w$) and the number of coil turns ($N$)



https://doi.org/10.1017/jmech.2012.104 Published online by Cambridge University Press

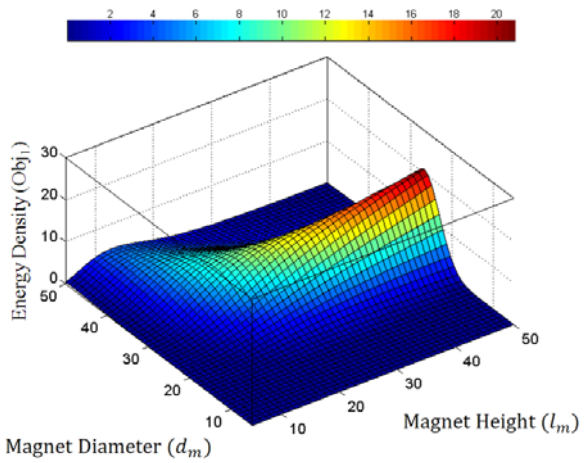



Fig. 14 Energy density ($OBJ_1$) with respect to the magnet's diameter ($d_m$) and height ($l_m$)

Table 2 Given data of the vibrating system and the vibration-based electromagnetic energy harvester

| Design Parameter | Given data |
|---|---|
| Mass of Permanent Magnet - $m$ | 0.0096kg |
| Mechanical Damping ratio by measured - $c_m$ | 0.028905N-sec/m |
| System Spring constant by measured - $k_{eq}$ | 260N/m |
| Residual Flux Density - $B_r$ | 1.2T |
| Excitation Input Amplitude - $Y$ | 0.06mm |

According to the results in section 7, based on the same excited amplitude, for various forcing frequencies, the resulting height of the coils are all lower than the height of the magnet. In addition, the magnet's height is also larger than its diameter. This is because the magnetic flux at the axis increases when the height of the magnet increases. Therefore, more layers of the coil can be wound along the magnet. Moreover, the total turns of the coil will also increase and the total electricity power will be raised when the smaller diameter of the enameled wire is adopted.

## 6. SIMULATED ANNEALING ALGORITHM

Evolutionary Algorithms have been widely developed for two decades. Many good EAs have been established. Simulated Annealing [13] is one of the best stochastic search methods. Here, sensitivity analyses is not necessary for choosing the starting design data, which is required in classical gradient methods of EPFM, IPFM and FDM [14]. Therefore, SA is adopted as an optimizer and used in the muffler's shape optimization.

The basic concept behind *SA* was first introduced by Metropolis *et al.* [15] and developed by Kirkpatrick *et al.* [16]. In this paper, the simulated annealing optimization method [17] has been used. The flow diagram for the SA method is depicted in Fig. 15. As indicated in Fig. 15, a new random solution ($X'$) will be chosen from the neighborhood of the current solution ($X$). If the change in the objective function (or energy) is negative, *i.e.*, $\Delta F \le 0$, a new solution will be acknowledged as the new current solution with the transition property $pb(X')$ of 1; if it is not negative, then the new transition property ($pb(X')$) varying from 0 ~ 1 will be calculated using the Boltzmann's factor ($pb(X') = \exp(\Delta F/CT)$) as shown in Eq. (14).

$$pb(X') = \begin{cases} 1, & \Delta F \le 0 \\ \exp\left(\dfrac{-\Delta F}{CT}\right), & \Delta F > 0 \end{cases} \tag{14a}$$

$$\Delta F = OBJ(X_n') - OBJ(X_n) \tag{14b}$$

where $C$ and $T$ are the Boltzmann constant and the current temperature. Additionally, compared to the new random probability of rand (0,1), if the transition property ($pb(X')$) is greater than a random number of rand (0,1), the new uphill solution, which results in a higher energy condition, will then be accepted; otherwise, it is rejected. The uphill solution at a higher temperature will therefore have a better chance of escaping from the local optimum. The algorithm repeats the perturbation of the current solution and the measurement of change in the objective function. Each successful substitution of the new current solution will lead to the decay of the current temperature as

$$T_{new} = kk \cdot T_{old} \tag{15}$$

where $kk$ is the cooling rate. The process is repeated until the predetermined number ($iter_{\max}$) of the outer loop is reached.

## 7. RESULTS AND DISCUSSION

The accuracy of the SA optimization depends on the $kk$ (cooling rate) and the $iter_{\max}$ (maximum iteration number). To investigate the influences of the above SA's control parameters, assessed ranges of the SA parameters are

$kk$ = (0.91, 0.92, 0.93, 0.94, 0.95, 0.96, 0.97, 0.98, 0.99); $iter_{\max}$ = (100, 200, 400, 800, 1000, 2000, 4000, 8000, 10000, 15000, 20000, 25000, 30000, 40000);

### 7.1 Results

For a base-vibrating system excited by a frequency of 10Hz, the optimal result by varying the SA's control parameters ($kk$, $iter_{\max}$) is shown in Table 3. As indicated in Table 3, the optimal design data can be obtained when the SA parameters at $kk$(0.95) and $iter_{\max}$



https://doi.org/10.1017/jmech.2012.104 Published online by Cambridge University Press

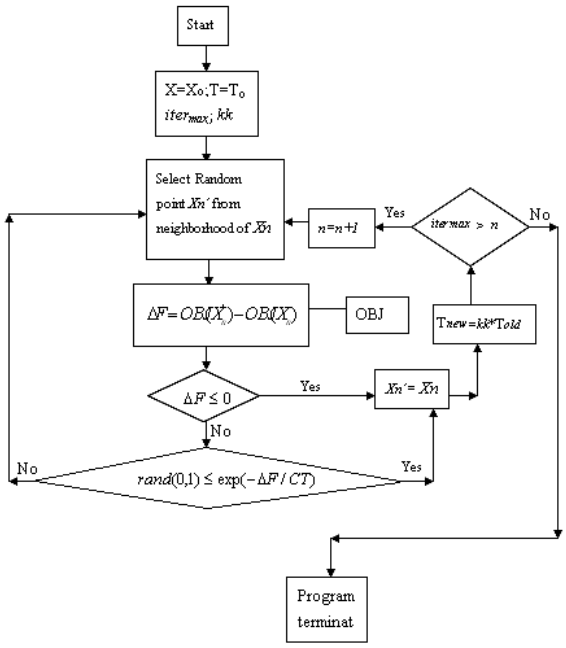



Fig. 15 Flow diagram of a SA optimization

Table 3 Optimal $OBJ_1$(J/kg) for the vibration-based electromagnetic energy harvester at various *kk* and $iter_{max}$ (targeted tone of 10Hz)

| SA control parameter | | design parameter | | | | result |
|---|---|---|---|---|---|---|
| *kk* | $iter_{max}$ | $l_m$ | $d_m$ | $N$ | $d_w$ | $OBJ_1$ J/kg |
| 0.91 | 100 | 42.008 | 20.671 | 91 | 0.125 | 0.737 |
| 0.92 | 100 | 16.155 | 29.949 | 123 | 0.106 | 0.455 |
| 0.93 | 100 | 20.565 | 43.182 | 89 | 0.242 | 0.205 |
| 0.94 | 100 | 44.961 | 30.310 | 105 | 0.299 | 0.192 |
| 0.95 | 100 | 34.977 | 44.211 | 179 | 0.125 | 1.243 |
| 0.96 | 100 | 22.822 | 36.175 | 110 | 0.157 | 0.453 |
| 0.97 | 100 | 49.937 | 34.747 | 122 | 0.183 | 1.042 |
| 0.98 | 100 | 8.173 | 7.701 | 334 | 0.410 | 0.000 |
| 0.99 | 100 | 5.207 | 29.310 | 212 | 0.665 | 0.000 |
| 0.95 | 200 | 36.889 | 31.418 | 127 | 0.158 | 0.843 |
| 0.95 | 400 | 49.132 | 30.489 | 112 | 0.186 | 0.938 |
| 0.95 | 800 | 40.954 | 41.203 | 181 | 0.120 | 1.457 |
| 0.95 | 1000 | 35.606 | 48.762 | 198 | 0.110 | 1.589 |
| 0.95 | 2000 | 43.461 | 36.012 | 161 | 0.130 | 1.237 |
| 0.95 | 4000 | 42.273 | 42.186 | 173 | 0.112 | 1.621 |
| 0.95 | 8000 | 48.053 | 42.829 | 167 | 0.136 | 1.660 |
| 0.95 | 10000 | 44.258 | 36.430 | 179 | 0.101 | 1.923 |
| 0.95 | 15000 | 43.607 | 45.625 | 202 | 0.107 | 1.933 |
| 0.95 | 20000 | 49.898 | 47.067 | 191 | 0.117 | 1.947 |
| 0.95 | 25000 | 49.131 | 45.273 | 203 | 0.111 | 2.020 |
| 0.95 | 30000 | 48.287 | 47.014 | 217.35 | 0.103 | 2.156 |
| 0.95 | 40000 | 48.287 | 47.014 | 217.35 | 0.103 | 2.156 |

(40000) are applied. Using the same control parameters (*kk*, $iter_{max}$) in the design data of the base-vibrating system excited with frequencies of 20Hz and 30Hz, the final simulated results with different excited frequencies (10Hz, 20Hz, and 30Hz) are shown in Table 4. As indicated in Table 4, the optimal $OBJ_1$ functions (energy density) with respect to various targeted excited frequencies (10Hz, 20Hz, and 30Hz) are 2.156J/kg, 11.733J/kg, and 30.305J/kg.

### 7.2 Discussion

For a base-vibration system excited with a specific frequency, a spring-mass electromagnetic energy harvester is attached to the base-vibration system. In the spring-mass electromagnetic energy harvester, a reciprocating vibrating motion of the permanent magnet occurs. Based on Faraday's law of electromagnetic induction and Lenz's law, the outputted electrical power of the coil will be induced. The fast motion of the magnet passing through the coil will result in higher electrical power. However, the damping ratio induced by the coil will increase and the related motion of the magnet will be retarded. Therefore, the mechanical system is coupled with the induced electrical power system. Moreover, the coil's damping ratio will be dominated by the coil turns ($N$), the magnet's height ($l_m$), the diameter ($d_m$), and the coil wire ($d_w$). Therefore, the investigation of the induced voltage with respect to these parameters is essential.

As discussed in Section 5, for a targeted excited frequency in the base-vibrating system, the response of the energy density ($OBJ_1$) with respect to the coil turns ($N$), the magnet's height ($l_m$), the diameter ($d_m$), and the coil wire ($d_w$) is very sensitive. Figure 12 indicates that the peak value of the energy density will increase when the excited displacement amplitude ($Y$) increases. Also, as indicated in Fig. 13, the energy density will increase when the diameter of the coil wire ($d_w$) decreases. Therefore, for a fixed height of coil ($l$), the number of coil turns will increase when the diameter of the coil wire decreases. Similarly, Fig. 14 indicates that the peak value of the energy density will increase when the magnet's height ($l_m$) increases and the magnet's diameter ($d_m$) decreases. Because of the primary distribution of the electromagnetic field along the axial direction of the magnet, the magnet's height ($l_m$) is more sensitive

Table 4 Comparison of the optimal energy density ($OBJ_1$) of the vibration-based electromagnetic energy harvester at three types of excited vibrating frequencies

| Case | Design parameter | | | | Result |
|---|---|---|---|---|---|
| | $l_m$ | $d_m$ | $N$ | $d_w$ | $OBJ_1$ (J/kg) |
| $f_{in}$ = 10Hz | 49.131 | 45.273 | 203 | 0.111 | 2.156 |
| $f_{in}$ = 20Hz | 49.956 | 41.778 | 229.700 | 0.112 | 11.733 |
| $f_{in}$ = 30Hz | 45.940 | 45.139 | 261.828 | 0.109 | 30.305 |



https://doi.org/10.1017/jmech.2012.104 Published online by Cambridge University Press

than the magnet's diameter ($d_m$). Moreover, as indicated in Fig. 11, the peak value of the energy density ($OBJ_1$) will occur when $d_m$ and $N$ increase or decrease simultaneously. Because the increment of coil turns ($N$) will simultaneously result in a higher induced electrical power and a larger damping coefficient, the appropriate coil wire ($d_w$) and coil turns ($N$) will be searched and a compromise will be found between the electrical power and the damping coefficient.

Moreover, as can been seen in Table 4, the optimal value of the energy density with respect to various targeted excited frequencies (10Hz, 20Hz, and 30Hz) is 2.156J/kg, 11.733J/kg, and 30.305J/kg. It is obvious that the captured electrical energy density will increase when the excited frequency of the base-vibrating system increases. This happens because the same excited amplitude of displacement and the higher frequency of vibration of the base will result in a higher inputted vibrating energy.

## 8. CONCLUSIONS

It has been shown that an SA can be used in the optimization of the vibration-based electromagnetic energy harvester within a limited space. The SA parameters such as the $kk$ (cooling rate) and the $iter_{\max}$ (maximum iteration number) play essential roles in the SA optimization. The higher $iter_{\max}$ will result in a better solution.

Based on Lenz's law, the outputted electrical power of the coil will be induced when the magnet moves across the region of the coil. Meanwhile, the damping ratio induced by the coil will increase and the related motion of the magnet will be retarded. Therefore, the mechanical system is coupled with the induced electrical power system. For a targeted excited frequency in the base-vibrating system, the energy density ($OBJ_1$) is closely related to coil turns ($N$), the magnet's height ($l_m$), the diameter ($d_m$), and the coil wire ($d_w$). Here, because of the primary distribution of the electromagnetic field along the axial direction of the magnet, the energy density ($OBJ_1$) will increase when the magnet's height ($l_m$) increases. Also, the increment of the coil turns ($N$) will simultaneously result in a higher induced electrical power and a larger damping coefficient. Therefore, the appropriate coil wire ($d_w$) and coil turns ($N$) will be searched for and a compromise between the electrical power and the damping coefficient will be found.

Moreover, the optimal value of energy density for various targeted excited frequencies (10Hz, 20Hz, and 30Hz) indicates that the extracted electrical energy density will increase when the excited frequency of the base-vibrating system increases.

Consequently, the approach used for the optimal design of the vibration-based electromagnetic energy harvester proposed in this study is quite efficient in maximizing the energy density ($OBJ_1$) within a space-constrained situation.


## ACKNOWLEDGEMENTS

The authors acknowledge the financial support of the National Science Council (NSC 100-2221-E-036-019), ROC.


## NOMENCLATURES

This paper is constructed on the basis of the following notations:

| | | |
|---|---|---|
| $A$ | : | cross section area of coil ($m^2$) |
| $A_c$ | : | cross section area of coil's wire ($m^2$) |
| $B$ | : | flux density (T/tesla) |
| $B_z$ | : | flux density at z-axis (T) |
| $c_e$ | : | electromagnetic damping coefficient of the coil(N-m $s^{-1}$) |
| $c_m$ | : | mechanical damping coefficient (N-m $s^{-1}$) |
| $c_{sys}$ | : | damping coefficient of vibration system (N-m $s^{-1}$) |
| $D_c$ | : | coil diameter (m) |
| $d_m$ | : | diameter of permanent magnet (m) |
| $D_s$ | : | spring diameter (m) |
| $d_s$ | : | diameter of the spring's wire (m) |
| $d_w$ | : | coil's wire diameter (m) |
| $iter_{\max}$ | : | maximal iteration in the simulated annealing method |
| $k_{sys}$ | : | spring constant of vibration system (N/m) |
| $kk$ | : | cooling rate in the simulated annealing method |
| $l$ | : | height of coil (m) |
| $l_c$ | : | length of a coil's wire (m) |
| $l_m$ | : | height of magnet (m) |
| $l_s$ | : | free length of the spring (m) |
| m | : | mass of permanent magnet (kg) |
| $N$ | : | number of coil's turns |
| $N_a$ | : | number of spring's turns |
| $OBJ_1$ | : | objective function for a energy density ($=V_{\text{total}}^2/(m \cdot R_{\text{total}})$) (J/kg) |
| $R_{load}$ | : | electrtical resistance of the loading of the electromagnetic energy harvester ($\Omega$) |
| $R_{iner}$ | : | electrtical resistance of the coil's wire ($\Omega$) |
| $V_o$ | : | peak voltage for the first period of time domain (volt) |
| $V_N$ | : | peak voltage for the $n$-th period of time domain (volt) |
| $V_{total}$ | : | total induce voltage |
| $Y$ | : | input amplitude for the exciting base (m) |
| $Z$ | : | relative displacement of a magnet with respect to the excited base (m) |
| $\rho_c$ | : | electrical resistivity coefficient of coil ($\Omega \cdot m$) |
| $\varsigma_{sys}$ | : | damping ratio of a vibration system |
| $\varsigma_m$ | : | damping ratio for a mechanical motion |
| $\varsigma_e$ | : | electromagnetic damping ratio |
| $\phi$ | : | magnetic flux (Wb) |
| $\delta$ | : | logarithm decrement value |
| $\varepsilon$ | : | induced voltage (Volt) |



https://doi.org/10.1017/jmech.2012.104 Published online by Cambridge University Press

## REFERENCES


1. Mitcheson, P. D., Green, T. C., Yeatman, E. M. and Holmes, A. S., "Architectures for Vibration-driven Micropower Generators," *Journal of Microelectromechanical Systems*, **13**, pp. 429–440 (2004).
2. Mitcheson, P. D., Yeatman, E. M., Rao, G. K., Holmes, A. S. and Green, T. C., "Energy Harvesting from Human and Machine Motion for Wireless Electronic Devices," *IEEE*, **96**, pp. 1457–1486 (2008).
3. Saha, C. R., O'Donnell, T., Loder, H., Beeby, S. and Tudor, J., "Optimization of an Electromagnetic Energy Harvesting Device," *IEEE Transactions on Magnetics*, **42**, pp. 3509–3511 (2006).
4. Constantinou, P., Mellor, P. H. and Wilcox, P., "Model of an Electromagnetic Vibration Generator," *Proceedings of the 41st International Universities Power Engineering Conference*, 2006. UPEC '06., **1**, pp. 6–10 (2006).
5. GlynneJones, P., "An Electromagnetic, Vibration-powered Generator for Intelligent Sensor Systems," *Sensors and Actuators A: Physical*, **110**, pp. 344–349 (2004).
6. Constantinou, P., Mellor, P. H. and Wilcox, P., "A Model of a Magnetically Sprung Vibration Generator for Power Harvesting Applications," *IEEE International Electric Machines & Drives Conference*, IEMDC'07., **1**, pp. 725–730 (2007).
7. McCarthy, K., Bash, M. and Pekarek, S., "Design of an Air-core Linear Generator Drive for Energy Harvest Applications," *Twenty-Third Annual IEEE Applied Power Electronics Conference and Exposition*, APEC pp. 1832–1838 (2008).
8. Li, H. and Pillay, P., "A Methodology to Design Linear Generators for Energy Conversion of Ambient Vibrations," *IEEE Industry Applications Society Annual Meeting*, IAS'08 (2008).
9. Saha, C. R., O'Donnell, T., Wang, N. and McCloskey, P., "Electromagnetic Generator for Harvesting Energy from Human Motion," *Sensors and Actuators A: Physical*, **147**, pp. 248–253 (2008).
10. Morais, R., Silva, N., Santos, P., Frias, C., Ferreira, J., Ramos, A., Simõesd, J., Baptista, J. and Reis, M., "Permanent Magnet Vibration Power Generator as an Embedded Mechanism for Smart Hip Prosthesis," *Procedia Engineering*, **5**, pp. 766–769 (2010).
11. Kimihiko, N., Takashi, S., Atsushi, N. and Tomohiro, K., "Portable Electrodynamic Generator Using Vibration on Walking Human Body," *Electromagnetics Symposium Proceedings*, **14**, pp. 347–350 (2002).
12. Stephen, N. G., "On Energy Harvesting from Ambient Vibration," *Journal of Sound and Vibration*, **293**, pp. 409–425 (2006).
13. Glover, F., "Heuristics for Inter Programming Using Surrogate Constraints," *Decision Sciences*, **8**, pp. 156–166 (1977).
14. Chang, Y. C., Yeh, L. J., Chiu, M. C. and Lai, G. J., "Shape Optimization on Constrained Single-Layer Sound Absorber by Using GA Method and Mathematical Gradient Methods," *Journal of Sound and Vibration*, **286**, pp. 941–961 (2005).
15. Metropolis, A., Rosenbluth, W., Rosenbluth, M. N., Teller, H. and Teller, E., "Equation of Static Calculations by Fast Computing Machines," *Journal of Chemical Physics*, **21**, pp. 1087–1092 (1953).
16. Kirkpatrick, S., Gelatt, C. D. and Jr., Vecchi, M. P., "Optimization by Simulated Annealing," *Science*, **220**, pp. 671–680 (1983).
17. Chang, Y. C., Chiu, M. C. and Liu, W. C., "Shape Optimization of One-chamber Mufflers with Perforated Intruding Tubes Using a Simulated Annealing Method," *Journal of Marine Science and Technology*, **18**, pp. 597–610 (2010).
18. Park, J. C., Bang, D. H. and Park, J. Y., "Micro-Fabricated Electromagnetic Power Generator to Scavenge Low Ambient Vibration," *IEEE Transactions on Magnetics*, **46**, pp. 1937–1942 (2010).
19. Bouendeu, E., Greiner, A., Smith, P. J. and Korvink, J. G., "Design Synthesis of Electromagnetic Vibration-Driven Energy Generators Using a Variational Formulation," *Journal of Microelectromechanical Systems*, **20**, pp. 466–475 (2011).
20. Mikolanda, T., "Study of Permanent Magnets Force Interaction," Ph. D Thesis, Technická Univerzita v Liberci, December 16th (2009).
21. Lallart, M., Anton, S. R. and Inman, D. J., "Design of a Frequency-Adjusting Device for Harvesting Energy from a Rotating Wheel," *Sensors and Actuators A*, **159**, pp. 196–203 (2010).
22. Lallart, M., Anton, S. R. and Inman, D. J., "Frequency Self-Tuning Scheme for Broadband Vibration Energy Harvesting," *Journal of Intelligent Material Systems and Structures*, **21**, pp. 897–906 (2010).


(Manuscript received October 18, 2011,
accepted for publication June 26, 2012.)



https://doi.org/10.1017/jmech.2012.104 Published online by Cambridge University Press